Battery Energy

WILEY

BATTERY ENERGY Open Access

RESEARCH ARTICLE OPEN ACCESS

Cross-Linked Acrylate Binder for High-Rate Graphite Anodes

Katarzyna Hofmann[1] | Anna Smith[2] | Norbert Willenbacher[1]

[1]Karlsruhe Institute of Technology, Institute for Mechanical Process Engineering and Mechanics, Karlsruhe, Germany | [2]Karlsruhe Institute of Technology, Institute for Applied Materials, Eggenstein-Leopoldshafen, Germany

Correspondence: Katarzyna Hofmann (katarzyna.hofmann@kit.edu)

Received: 11 July 2025 | **Revised:** 8 September 2025 | **Accepted:** 10 October 2025

Funding: The study was supported by the Deutsche Forschungsgemeinschaft (WI 3138/33–1).

Keywords: graphite anodes | lithium-ion batteries (LIB) | polyacrylic acid (PAA) | polymeric binders

ABSTRACT

Sodium carboxymethyl cellulose (CMC) and polyacrylic acid (PAA) are state-of-the-art binders in aqueous-processed anodes for lithium-ion batteries. Binders act as dispersing agents and rheology modifiers in aqueous slurries, while also providing mechanical integrity of dry electrodes during battery fabrication and operation. However, despite their low concentration, they may have detrimental effects on the conductivity and electrochemical performance of batteries, for example, due to their adsorption on active material particles, which is supposed to limit Li^+ insertion and extraction, but also affect electrode microstructure and adhesion to the current collector. Here, a commercially available, cross-linked acrylate binder (Carbopol® Ultrez10, x-PAA) with high thickening efficiency is applied for graphite anodes. At lower polymer content, anode slurries based on x-PAA exhibit high-shear viscosities similar to those of the CMC reference and provide a yield stress, which is advantageous for slurry stability. Furthermore, SBR content could be reduced without loss of adhesion strength compared to the CMC reference, since x-PAA does not adsorb onto graphite. Thus, the total binder content could be lowered by about 40% in comparison to reference anodes comprising CMC. The substantial reduction in total binder amount resulted in slightly lower long-term stability compared to the reference cell including CMC. Cells incorporating x-PAA, however, outperformed references under fast-charging conditions (up to 5C) presumably since x-PAA does not adsorb on graphite, thus enabling more effective Li^+ insertion and extraction. Further refinement of crosslinking microstructure may enable fabrication of electrodes with higher energy density and higher capacity retention during cycling, irrespective of cycling rate.

1 | Introduction

Aqueous processing represents the state-of-the-art in anode production for lithium-ion batteries (LIBs). The primary advantage of this method is its environmental friendliness and cost-effectiveness, as it does not require the use of hazardous and expensive organic solvents or the subsequent solvent recovery equipment during electrode manufacturing [1, 2]. To guarantee the adequate dispersion of all electrode slurry components while maintaining suitable flow properties for the coating process, polymeric binders are incorporated into the formulation. Additionally, they facilitate the mechanical integrity of electrodes during both fabrication and operation [3–5].

Carboxymethyl cellulose (CMC), polyacrylic acid (PAA), and styrene butadiene rubber (SBR) are among the most commonly used water-based binders for LiB anodes. CMC and PAA primarily act as dispersing agents and rheology modifiers, facilitating uniform particle distribution in the slurry and providing the flow behavior demanded for high-quality uniform

coating. At higher molecular weights, these polymers can also improve cohesion of the electrode layer [6, 7]. According to the literature, both linear PAA and CMC adsorb onto active material particles, and the underlying adsorption mechanisms depend, among other factors, on the type of active material. For natural graphite, which possesses a relatively smooth surface, linear PAA and CMC predominantly adsorb onto the basal planes through hydrophobic interactions [8–10]. In contrast, for artificial graphite, natural graphite with defective surfaces, or silicon, adsorption occurs primarily via interactions of the polymers' carboxylic groups with surface functionalities of the active material particles [9–12]. PAA's advantageous properties as an electrode binder include its higher carboxylic group density compared to that of CMC, which facilitates enhanced interaction with active material particles such as silicon, as well as low swelling in carbonate-based electrolytes [7, 13, 14].

To increase the energy density of a LIB, it is desirable to minimize the binder content, as it constitutes an electrochemically inactive component of an electrode. However, even more importantly, despite their low concentration, binders may have a detrimental effect on the conductivity and electrochemical performance of battery electrodes. CMC adsorbs onto graphite, which reduces the adhesion between the anode and the current collector, and also affects the electrode microstructure depending on molecular weight and degree of substitution [6, 15]. Linear PAA poses significant limitations regarding the control of rheological properties. Specifically, the thickening efficiency of this polymer at the molecular weights typically used in LIB applications (250–450 kDa) is poor. Consequently, elevated binder concentrations are necessary to attain a slurry with adequate flow properties for coating processes. Moreover, the viscosity of PAA solutions is highly pH-dependent [16], in contrast to CMC, which offers more stable behavior [17]. In addition, the glass transition temperature of both PAA and CMC exceeds 100°C [18, 19], which is far above the typical operating temperature range of LIBs (−20°C to 55°C) [20]. Consequently, these polymers remain brittle under the conditions experienced during battery operation [21]. This brittleness limits the potential for binder content reduction, as an additional adhesion promoter is still necessary to ensure adequate bonding between the electrode layer and the current collector foil. Accordingly, SBR with a glass temperature typically ranging between −10°C and 10°C is mainly employed as an adhesion promoter, but also enhances anode cohesion [22].

Numerous examples of the application of linear PAA as a binder, particularly for silicon-containing anodes, can be found in the literature [7, 13, 23, 24]. However, as previously stated, due to the low viscosity of PAA, it is necessary to employ a binder amount exceeding 10 wt% or to incorporate an additional thickener, for example, sodium alginate [25], to achieve the desired dispersion properties. To enhance the mechanical properties of PAA and introduce new functionalities such as ionic and electronic conductivity, next-generation PAA binders are designed with two-dimensional (2D) or three-dimensional (3D) architectures [26]. These structures are achieved through grafting or cross-linking with other polymers, including carboxymethyl cellulose (CMC) [27], poly(vinyl alcohol) (PVA) [28], chitosan [29, 30], sodium alginate [31], gum arabic [32], and others.

For example, Preman et al. [33] recently introduced a novel binder for silicon anodes, x-PAA/PSUOH, formed by cross-linking PAA with a synthesized copolymer of poly(sodium 4-styrenesulfonate-co-ureido-pyrimidinone methacrylate-co-hydroxyethyl methacrylate). Anodes incorporating the x-PAA/PSUOH binder exhibit enhanced mechanical integrity and ionic conductivity, achieving an initial capacity of 3572 mAh g^{-1} and a capacity retention of 71% over 300 cycles. Jeong et al. [34] cross-linked highly elastic poly(urea-urethane) (PUU) with rigid PAA and employed the resulting copolymer as an anode binder for Si electrodes. By combining the distinct mechanical properties of both polymers, the structural integrity of the Si anode was maintained despite its large volume expansion during cycling. Consequently, the cells exhibited enhanced cycling performance compared with those using the neat PAA binder. Similarly, Wang et al. [35] designed a self-healing PCI binder through chemical cross-linking of PAA, polyethyleneimide (PEI), and citric acid (CA). The binder, rich in carboxyl and amide groups, strongly interacts with Si nanoparticles and exhibits excellent elasticity along with high adhesive strength. As another example, Lv et al. [36] synthesized a cross-linked network binder based on ultraviolet (UV)-cured waterborne polyurethane acrylate (WPA) for Si/C anodes. The high cross-link density enhanced mechanical strength and significantly reduced electrolyte swelling. Combined with the binder's high electronic and ionic conductivity, this resulted in improved cycling stability compared with PAA-based cells.

Despite these promising properties, such modified PAA binders have not yet reached commercialization. This is primarily due to the complexity of the synthesis process, which involves multiple steps, yields limited quantities, finally resulting in high production costs.

Recently, we demonstrated that polymer adsorption on graphite and silicon active material impedes strong SBR-particle bonding, thereby reducing the overall adhesion of the anode to the copper current collector [15]. Building on these findings, the present work explores the application of a commercially available, highly cross-linked acrylate thickener Carbopol® Ultrez10, which, in combination with SBR, forms an efficient binder system for graphite anodes.

Carbopol® Ultrez 10 is a highly cross-linked polyacrylic acid polymer (Figure 1) composed of acrylic acid homopolymers and copolymers with alkyl acrylates, with crosslinking provided by allyl ether derivatives of polyalcohols. As a commercially available rheology modifier and thickener, it is widely used, for example, in cosmetics, pharmaceutical formulations, or coatings [37, 38]. When dispersed in water, Ultrez 10, even at low concentrations, forms gels with a very high elasticity, which strongly depends on the pH [39]. At concentrations relevant for technical applications (0.1%–0.5 wt%), Ultrez 10 exhibits a highly heterogeneous microstructure composed of agglomerates of primary gel particles, forming a percolated network in the neutralized state. The crosslink density of these gel agglomerates is nonuniform, and they are surrounded by loosely associated polymer chains that extend outward. A comprehensive study of the microstructure of Ultrez 10 is provided in [37].

In this study, we demonstrate that graphite electrodes based on Ultrez 10 and SBR binder exhibit excellent rate capability

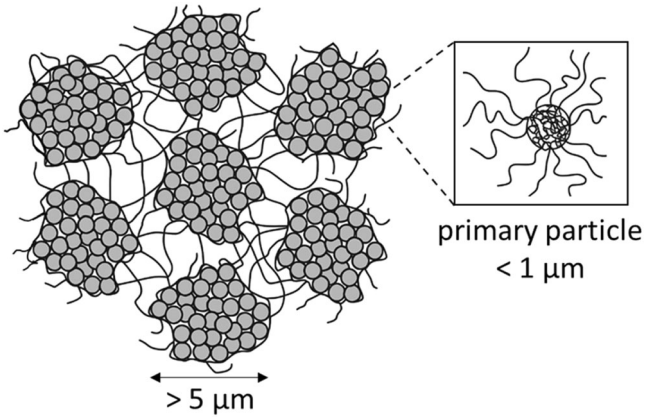

FIGURE 1 | Schematic illustration of the x-PAA binder microstructure. The inset shows a primary particle with a highly cross-linked core and dangling ends. Edited from [37]. PAA, polyacrylic acid.

and stable long-term cycling performance. Moreover, due to the very high thickening efficiency of Ultrez 10 and the lack of adsorption on graphite particles, a 38% reduction in total binder content could be achieved compared to a reference electrode including a conventional CMC/SBR binder system.

2 | Experimental

2.1 | Electrode Preparation

The preparation of water-based anode slurries always began with the formulation of a binder solution. Three different polymers were used: highly cross-linked polyacrylic acid x-PAA Carbopol® Ultrez 10 (Lubrizol, USA), linear polyacrylic acid (l-PAA) with molecular weight $M_w = 250$ kDa, Sigma-Aldrich, Germany), and sodium carboxymethylcellulose (CMC) with $M_w = 150$ kDa and degree of substitution DS = 0.7 (TEXTURECELL CRT 2000PA07, DuPont, USA). x-PAA, and CMC were utilized in powder form, while the l-PAA was employed as a 35% aqueous solution.

For x-PAA, the first step of solution preparation was to produce a stock solution of 1 wt% by gradually introducing the polymer powder into a beaker containing distilled water, with continuous gentle agitation applied throughout the process. Stirring was performed using a propeller with a diameter d of 50 mm, operating at 400 rpm for 30 min, followed by 100 rpm for an additional 30 min. Subsequently, the polymer solution was subjected to continuous stirring using a magnetic stirrer for approximately 12 h. Then, the final binder solution (0.5 wt % and 0.7 wt%) for a slurry was prepared by first diluting the stock solution with distilled water and subsequently neutralizing it with NaOH. The initial pH of the x-PAA solution was approximately 2, and after neutralization, it increased to around 6.

Similarly, a l-PAA solution was prepared by first diluting a specific amount of a 35 wt% aqueous l-PAA solution with distilled water, followed by stirring with a 50 mm diameter propeller at 1200 rpm for 30 min. The initial pH value of the resulting solution was approximately 2, and was subsequently modified to a value of about 6 using NaOH.

A CMC solution was prepared by dissolving CMC powder in a beaker containing distilled water. The components were stirred using a 50 mm diameter propeller at 1200 rpm for 30 min until complete powder dissolution. The resulting CMC solution had a pH value of about 7.

All final binder solutions were formulated to contain 95% of the total amount of distilled water required for slurry preparation. In the subsequent steps, the powder components were admixed to the binder solution: carbon black (C-Nergy Super C65, Imerys Graphite & Carbon, Switzerland) was added first, followed by graphite (SMG A5, Showa Denko Materials Co Ltd., Japan). The mixture was then stirred using a dissolver ($d = 50$ mm) at 2000 rpm for 5 and 10 min, respectively. Next, styrene butadiene rubber (SBR, BM-451B, Zeon, Japan) as 40 wt% aqueous dispersion was introduced and stirred at 2000 rpm for 5 min. Finally, the remaining 5% of distilled water was added and the slurry was mixed at 2000 rpm for another 5 min. All slurries maintained a constant solids content of 42 wt% (corresponding to 25 vol%).

After the mixing process, slurries were degassed in a desiccator and subsequently coated on a 10 µm thick copper foil (SE-Cu, Schlenk Metallfolien GmbH & Co. KG, Germany) using a doctor blade (ZUA 2000, Zehntner GmbH, Switzerland). The coating was performed at a velocity of 10 mm s^{-1}, with a coating gap of 160 µm for anodes with x-PAA, and 180 µm for anodes with CMC and L-PAA. The thickness of the dried electrodes was found to range from 69 to 72 µm, with porosity measuring approximately 60%. Some of the dried anodes were calendered with a roll-to-roll calendar (GKL, Saueressig GmbH, Germany) with a roll width of 400 mm and a working speed of 1 m min^{-1} to achieve a target porosity of 40%.

2.2 | Rheological Characterization of Anode Slurries

The rheological properties of anode slurries were characterized using a rotational rheometer (Physica, MCR 501, Anton Paar 201 GmbH, Germany) equipped with a plate-plate measuring system (PP25TG, diameter $d = 25$ mm, gap height $h = 1$ mm). Steady shear measurements were performed in a logarithmic shear stress ramp mode, covering the stress range from 0.01 to 1000 Pa with 10 points per decade and a logarithmic decreasing measuring time from 60 s to 10 s. Measurements were performed at 20°C.

2.3 | Mechanical Properties of Anodes

Anodes, both before and after the calendering process, as well as after electrochemical cycling, underwent 90°-peel tests using a universal testing machine (Texture Analyser TA.XT plus, Stable Micro Systems, UK) equipped with a 5 kg load cell. For testing, anodes were first cut into 2.5 cm wide strips and affixed to a movable test plate using double-sided adhesive tape. The

free end of a sample was attached to the machine arm at a 90° angle and subsequently peeled off at a constant velocity of 5 mm s^{-1}. To ensure reproducibility, at least 10 samples of each anode formulation were tested. The peel force was recorded for each sample, normalized to the sample width, and averaged to obtain the line load.

Furthermore, to determine the cohesion of anode layers, degassed slurries were cast into silicone molds and dried at 50°C for approximately 18 h. The dried samples were then cut and ground into cubes measuring 5 × 5 mm using sandpaper. These samples were subsequently subjected to compression tests in accordance with the DIN 51104 standard, employing a universal testing machine (Texture Analyzer TA.XT plus, Stable Micro Systems, UK) equipped with a 50 kg load cell.

2.4 | Electrochemical Characterization of Anodes

2.4.1 | Pouch Cell Assembly

Calendered anodes with a target capacity of 2.1 mAh cm^{-2} were punched with size of 5.4 × 5.4 cm and paired with one-sided coated commercial NMC111 ($LiNi_{0.33}Mn_{0.33}Co_{0.33}O_2$) cathodes with an areal capacity of 1.9 mAh cm^{-2} punched with size 5.0 × 5.0 cm. Electrodes and 5.9 × 5.9 cm PET-based separators with a ceramic coating were dried under vacuum for 24 h at 130°C and 180°C, respectively. Subsequently, the assembly of lab-scale pouch cells was conducted using a semi-automated manufacturing line under dry room conditions. The cells were filled with 450 μL electrolyte (1 M $LiPF_6$ in 50/50 (w/w) ethylene carbonate (EC) and dimethyl carbonate (DMC) with 3 wt% of vinylene carbonate (VC) as an additive (already mixed, purchased from Gotion) and sealed under reduced pressure. Subsequently, the cells were stored over night at 40°C for sufficient wetting of the separator and electrodes.

For each anode formulation, two cells were built and after formation subjected to the rate capability test in discharge direction, followed by the cycling test including RiDCs. Additionally, two cells containing CMC anodes and two cells with x-PAA anodes were assembled, formatted and tested in the rate capability test in charging direction.

2.4.2 | Data Acquisition

Electrochemical testing was performed using BaSyTec CTS LAB instruments while cells were stored in a climate chamber at 25°C (±0.1°C).

2.4.3 | Formation

For the formation step four cycles were applied, where charging was performed with constant current (CC) at C/10 until a voltage of 4.2 V was reached with subsequent charging at constant voltage (CV) until the current dropped below C/20. The discharge was performed using CC of C/10. Finally, the cells where charged to 3.7 V using C/10 CC for storage until the next cell test was performed.

2.4.4 | Rate Capability Test

An asymmetric rate test was performed in probing either discharge or charge capability. For discharge testing charging was done with a C-rate of C/2 CC including a CV phase at 4.2 V (until I < C/20) and rates in discharge direction were varied from C/2 to 5C until a cut-off voltage of 3.0 V. To check for degradation due to the rate testing C/2 discharge was included at the end of the test procedure. For each C-rate two full cycles were applied.

For charge capability same rates were used, however, now the discharge current was kept constant applying C/2 CC and charging was varied from C/2 CC to 5C CC and back to C/2 (each two cycles). All charging steps ended with CV-phases (until I < C/20). For the rate testing in charge direction values from the CC-charging phase are plotted as they represent the true power capability of the battery cell.

2.4.5 | Cycling Test Including Direct Current Internal Resistances (RiDCs)

For long term cycling, all cells were cycled applying 1C CC with CV until I < C/20 and 1C CC discharge current. The voltage window was 3.0–4.2 V. "Check-up cycles" were used every 100 cycles meaning measurements were made at five states of charge (SOCs), namely 10%, 30%, 50%, 70%, and 90%, based on the determined cell capacity just before the test. For all SOCs RiDC were determined by use of current pulses of 1C in discharge direction for 20 s. Applying Ohm's law, the DC internal resistances were determined using the potential drop (difference between the potential at the end of the pulse and the potential in rest state before the pulse) and the applied current for the respective pulses.

2.5 | Post-Mortem Analysis

After electrochemical testing, cells were discharged to minimal voltage of 3.0 V and held for 4 h using a CV-phase. Under dry-room atmosphere pouch bag cells were then opened to examine the surfaces of the electrodes and separators by optical analysis using a light microscope (OLYMPUS BX53 M, Japan).

3 | Results and Discussion

3.1 | Slurry Rheology

This section highlights the superior thickening properties of x-PAA. The objective was to adjust the flow behavior of the x-PAA slurry, particularly at high-shear rates, which are relevant for the coating process, to that of the CMC reference slurry.

The x-PAA solutions were neutralized to a pH of approximately 6, that is, close to that of the CMC solution to avoid additional electrochemical effects. At this point, Carbopol® agglomerates undergo swelling, resulting in the formation of a sample spanning network, which is responsible for the observed superior thickening properties [37] and the gel-like texture.

Anode slurries with two different x-PAA concentrations (0.27 vol% and 0.37 vol%, which correspond to 0.29 wt% and 0.40 wt%, respectively) were prepared, and Figure 1 illustrates their viscosity as a function of shear rate. Due to the network provided by the x-PAA binder, these slurries exhibit a yield stress of about 4 Pa and 29 Pa, respectively, and shear thinning behavior at higher stresses. In contrast, the reference slurry with 0.58 vol% (0.72 wt%) CMC does not exhibit a yield stress and shows shear thinning throughout the whole investigated shear stress range, as expected since the CMC itself does not form a gel and, moreover, partially adsorbs onto the graphite particles thus providing steric stabilization of the dispersed particles. The nonadsorbing CMC fraction, however, thickens the continuous phase and controls the viscosity of the slurry [40–42]. Note that, in contrast to CMC and l-PAA, x-PAA does not adsorb onto graphite particles, as confirmed by IR spectroscopy (Supporting Information: Figure S1), and therefore cannot contribute to their steric stabilization. The absolute value of the yield stress is thus determined not only by the strength of the x-PAA network, but also by the particle network created due to prevailing van der Waals attraction. The high shear viscosity of the slurry containing 0.40 wt% x-PAA closely matches that of the reference slurry and was thus selected for fabrication and characterization of electrodes, which will be discussed below. This result demonstrates that equivalent rheological performance can be achieved with up to 36% less polymer, highlighting the superior efficiency of the x-PAA as an anode binder.

Moreover, the x-PAA slurry exhibits a significant yield stress, which prevents or slows down sedimentation of graphite particles in the water-based slurry, thus providing an extended shelf-life, and facilitates efficient pumping [43–46]. It further enables the formation of well-defined coating edges [47] and also reduces crack formation during fast drying of thick electrode layers. Another advantage is that the yield stress significantly suppresses binder migration—a major concern under high-rate drying conditions that can lead to uneven binder distribution and, as a consequence, to inferior mechanical, electrical, and electrochemical properties of the electrode [48–50].

For comparison, the flow behavior of a second, l-PAA based reference slurry was also investigated (see Figure 2). The l-PAA slurry comprises 3.10 vol% (3.41 wt%) of polymer, which is considerably higher than the polymer content in both the CMC and x-PAA slurries. Despite its high polymer content, the l-PAA slurry exhibits a markedly lower yield stress of only 1.3 ± 0.3 Pa compared to the x-PAA slurry including 0.37 vol% polymer. Beyond this critical stress, the shear viscosity is nearly Newtonian (i.e., independent of the applied shear stress) and much lower than for the CMC and higher concentrated x-PAA slurry (0.37 vol%). Consequently, the particles in the l-PAA slurry are not sufficiently stabilized over time, which is supposed to result in detrimental effects during technical scale storage and processing operations.

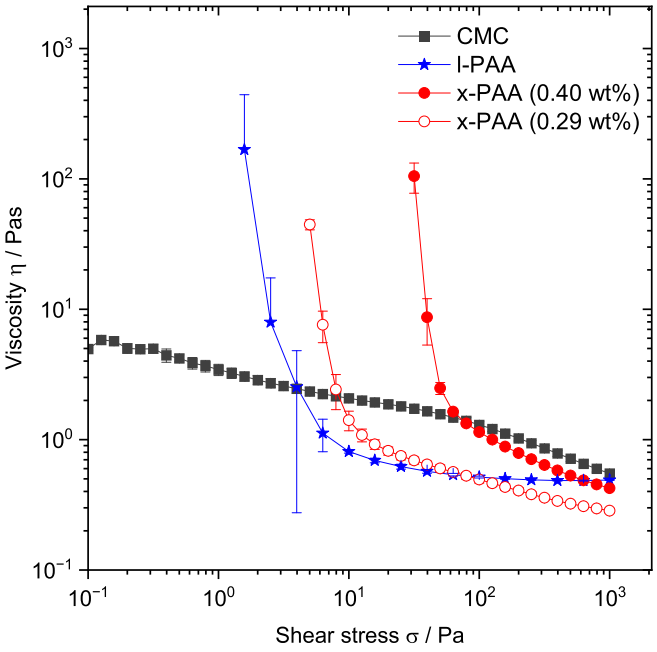

FIGURE 2 | Viscosity η as a function of shear stress σ for graphite slurries with solids volume fraction $\varphi = 25$ vol% and different binders: CMC/SBR (black squares), l-PAA/SBR (blue stars), and x-PAA/SBR with 0.40 wt% x-PAA and 0.29 wt% x-PAA (red closed and open circles, respectively). PAA, polyacrylic acid; SBR, styrene butadiene rubber.

3.2 | Mechanical Properties of Anodes

The second approach to reduce the total binder content is based on previous investigations demonstrating the fraction of CMC binder adsorbed on the active material particles diminishes the adhesion between these particles and the current collector [15]. Accordingly, a non-adsorbing polymer binder should allow for a reduced addition of SBR without loss in adhesion.

As expected, using non-adsorbing x-PAA as an anode binder, while maintaining a SBR concentration (2.87 wt% in the dry anode layer) similar as in the CMC reference anode, results in a substantial improvement of adhesion strength (Figure 3). Accordingly, the SBR content in the x-PAA slurry was reduced to 1.87 wt% in dry anode layer, the amount at which the line load of the anode layer prepared from the x-PAA slurry was similar to that of the CMC reference. However, the comparison of the absolute line load values has to be treated carefully. The pictures of corresponding electrode samples after peeling, reveal that the CMC-based electrode exhibits purely adhesive failure, whereas the presence of numerous particle residues on the peeled x-PAA anode samples indicates that in this case cohesive failure dominates (Supporting Information: Figure S2). Finally, we have prepared an l-PAA-based electrode including 8.28 wt% linear PAA and 1.87 wt% SBR, which exhibits similar line load as the CMC-based electrode.

The lower cohesion of x-PAA electrodes was confirmed via compression tests on dry anode layers; corresponding results are shown in Figure 4. As known from literature, an increased content of either thickening agent (e.g., CMC or PAA) [6] or adhesion promoter (e.g., SBR) [22] correlates with elevated electrode cohesion. Accordingly, the x-PAA anodes with the

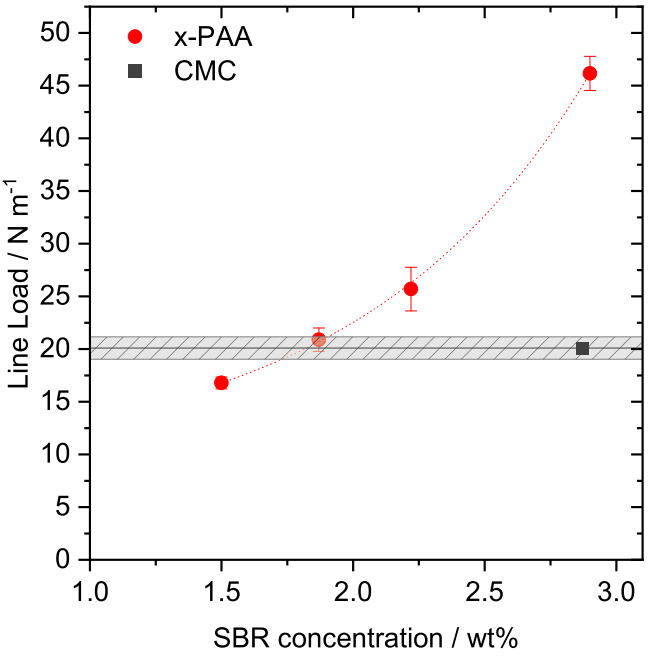

FIGURE 3 | Line load of non-calendered anodes with 0.98 wt% x-PAA and various amounts of SBR (red circles). The polymer concentrations refer to the dry anode layer. The black square and black hatched area indicate the line load of the non-calendered CMC reference anode. The thickness of all negative electrodes was about 65 µm. CMC, carboxymethyl cellulose; PAA, polyacrylic acid; SBR, styrene butadiene rubber.

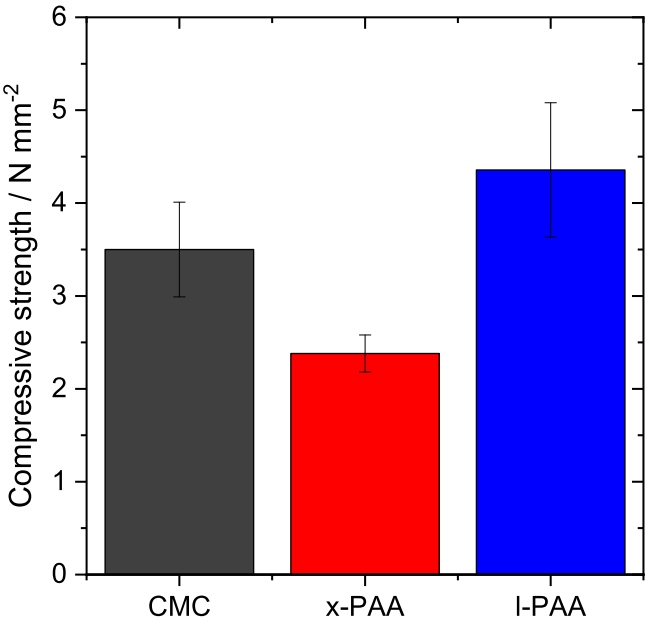

FIGURE 4 | Compressive strength of thick anode layers comprising different binders: CMC, x-PAA, and l-PAA. Composition of the different dry anode samples is provided in Table 1. CMC, carboxymethyl cellulose; PAA, polyacrylic acid.

lowest total binder content of 2.86 wt% demonstrate the lowest level of cohesion, whereas the l-PAA samples with a more than three times higher binder content of 9.93 wt% exhibit the highest cohesive strength. Consequently, anodes that employ CMC as a binder, with a content of 4.62%, show an intermediate degree of cohesion. The total amount of binder in the electrode layers directly correlates to their cohesive strength, which also affects the line load determined in peel experiments. In conclusion, a non-adsorbing binder with high thickening efficiency, such as x-PAA, allows for a reduction of the binder content itself, and additionally for the reduction of SBR without loss of adhesion, but this is limited by the corresponding loss in cohesion.

Based on the rheological and mechanical characterization described above, we have prepared three slurries for electrode fabrication, including CMC, x-PAA, or l-PAA, as well as SBR as binders. The composition of the corresponding electrodes is provided in Table 1.

The dry anode made from the x-PAA slurry has a total binder content of 2.86 wt%, which is 38% lower compared to the CMC reference anode.

3.3 | Anode Performance Within a Full-Cell Battery Configuration

To compare the anode performance in a full-cell configuration, CMC, x-PAA, and l-PAA anodes were paired with commercial NMC111 cathodes with the areal capacity of 1.9 mAh cm^{-2}. Due

TABLE 1 | Composition of anodes containing CMC, l-PAA, and x-PAA binders selected for electrochemical performance tests. All concentrations refer to the dry anode layer.

Anode	CMC	l-PAA	x-PAA
Graphite, wt%	93.45	84.62	96.01
Carbon Black, wt%	1.93	1.75	1.98
Thickener, wt%	1.75	8.28	0.98
SBR, wt%	2.87	1.65	1.87
Total binder content, wt%	**4.62**	**9.93**	**2.86**

Abbreviations: CMC, carboxymethyl cellulose; PAA, polyacrylic acid; SBR, styrene butadiene rubber.

to the full-cell balancing aspects [51] the target areal capacity of anodes was approximately 2.1 mAh cm^{-2}. All electrochemical tests were carried out on two cells for each anode composition. After formation, which included 4 charging/discharging cycles with C/10, anodes with CMC and x-PAA exhibited very similar practical discharge capacities (4th cycle) of about 44.5 mAh (Table 2), whereby anodes with l-PAA showed slightly lower capacity of 43.1 mAh.

At first, asymmetric discharge rate capability tests of the pouch cells (delithiation capability of the anode) were performed using a constant charging rate of C/2, followed by a constant voltage phase with a current limit of I < C/20. Discharging was carried out at varying rates ranging from C/2 to 5 C. Figure 5a illustrates the results in terms of absolute discharge capacity retention. The rate performance of anodes containing l-PAA is noticeably poor. From 2 C onwards, a significant decrease in absolute capacity is observed with increasing C-rate, compared to CMC and x-PAA anodes. The retained cell capacity at 3 C is 35.5 mAh (which is 84.5% of the initial capacity), whereas for

TABLE 2 | Absolute and areal practical capacities of full cells including anodes with CMC, l-PAA, and x-PAA binders after the fourth discharge formation cycle.

Cell properties	CMC	l-PAA	x-PAA
Absolute capacity, mAh	44.56 ± 0.13	43.11 ± 0.03	44.45 ± 0.07
Graphite mass loading, mg cm^{-2}	6.0	5.9	5.8
ICE, %	87.4	87.0	85.9

Abbreviations: CMC, carboxymethyl cellulose; ICE, initial coulombic efficiency; PAA, polyacrylic acid.

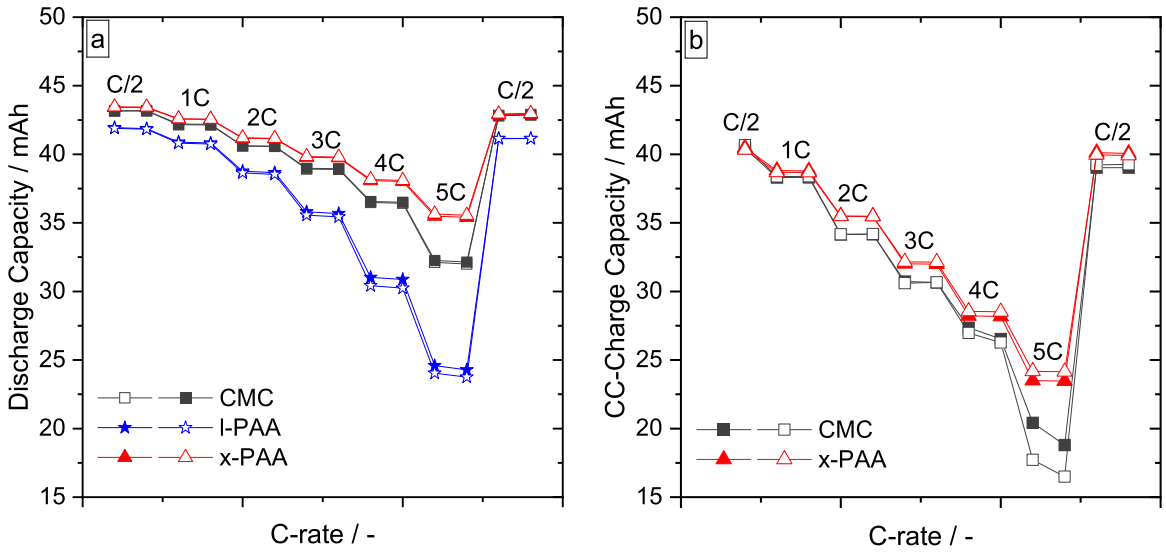

FIGURE 5 | Absolute discharge (a) and CC-charge (b) cell capacities as a function of dis-/charge C-rate for pouch cells containing CMC, l-PAA and x-PAA anodes. CC, constant current; CMC, carboxymethyl cellulose; PAA, polyacrylic acid.

anodes with CMC and x-PAA 39.0 mAh and 39.8 mAh, which is 90.3% and 91.6% of the initial capacity, respectively. Also, at higher C-rates the difference between cells containing anodes with CMC and x-PAA becomes apparent. While at 3 C CMC anodes exhibit 39 mAh and x-PAA anodes 39.8 mAh, at 4 C the difference is significant: 36.6 mAh and 38.2 mAh, and at 5 C 32.2 mAh and 35.6 mAh, which is 74.7% and 82.0% of the initial capacity, respectively. At the last C/2 step cells with CMC and x-PAA anodes demonstrate nearly 100% of their initial capacity, indicating that no irreversible degradation occurred. In the case of anodes with l-PAA the retained capacity in the last C/2 step achieves 41.1 mAh, which is about 98% of the initial capacity. These results were expected, since anodes with l-PAA contain the highest amount of electrochemically inactive binder material. This increases the resistance of the anode and consequently the internal resistance of the cell. Such an increase in internal resistances leads to voltage limits being reached more rapidly, which reduces the amount of usable charge during discharge and ultimately lowers the cell's effective capacity. Anodes containing x-PAA have the lowest binder content and thus the lowest internal resistance, resulting in an overall better rate capability compared to the CMC and l-PAA reference anodes. The correlation between rate capability and anode resistance is further supported by the shift of the voltage plateau, e.g., decrease of voltage values in the discharge direction with increasing resistance. A plot with selected voltage profiles for the C-rates C/2 and 5 C for the CMC, x-PAA and l-PAA cells is shown in the Supporting Information. The same trends, which can be seen in Figure 5a for rate capabilities, are also evident in the voltage shifts for all C-rates, with the most pronounced difference occurring at 5 C, as expected (Supporting Information: Figure S3). Furthermore, direct current internal resistances (RiDC) values, which are presented in Figure 7b and will be discussed in detail below, support this trend.

In the next step, x-PAA anodes were compared with CMC anodes in terms of rate capability in the charging direction. Therefore, another set of pristine anodes were assembled in pouch cells, and an asymmetric rate capability test was performed at a constant discharging rate of C/2 and varying charging rates ranging from C/2 to 5 C. At lower C-rates, CMC and x-PAA anodes show no differences in capacity retention (Figure 5b). However, for higher currents starting from 2 C, CMC anodes exhibit lower absolute constant current (CC) capacities in comparison to x-PAA anodes. At 5C the difference between absolute capacities is the highest, 23.5 mAh and about 19 mAh for x-PAA and CMC, respectively, which is 58% and about 45% of the relative capacity of x-PAA and CMC anodes, respectively. Also, it can be noted that at 4C and 5C CMC-based anode cells show some irreproducible behavior as the repeated charge test does not retain the capacity of the first cycle. This might already indicate some degradation. At the final step of the rate capability test, the cells were charged with C/2 again. It can be observed that cells with x-PAA anodes almost completely recover (99% capacity retention), whereas cells with CMC anodes lost irreversibly about 3.5% of their initial capacity.

The superior charging rate capability of x-PAA anodes might originate from the absence of an adsorbed polymer layer on the graphite particles, which enables direct contact with the electrolyte. This results in minimal interfacial resistance, thereby facilitating more efficient Li^+ insertion and extraction as the graphite surface remains unobstructed [52]. In contrast, CMC anodes exhibit diminished rate performance, likely due to the presence of a blocking polymer layer on the graphite surface.

Subsequently, the cells were disassembled in discharged state (delithiation of anode) and subjected to visual inspection to assess potential degradation effects. A substantial accumulation of particle residue can be observed on the separators, particularly in cells incorporating anodes with CMC (Figure 6). In contrast, separators from cells containing x-PAA exhibit considerably less residue. Examination under a light microscope reveals a distinct difference in the nature and extent of the deposits. Specifically, separators from CMC cells displayed evidence of lithium plating, characterized by silver-grey deposits [53]. In comparison, separators from x-PAA cells show no signs of lithium plating, with only minor particulate graphite and/or carbon black residue present.

Long-term cycling was conducted on pouch cells following the rate capability test in the discharge direction, using a 1 C charge and 1 C discharge protocol. Every 100 cycles, a check-up cycle (C/10) was performed. Figure 7a illustrates the long-term cycling performance, displaying the capacity evolution over 1000 cycles for two cells of each anode formulation. The CMC anodes demonstrate superior electrochemical performance in terms of capacity retention, retaining approximately 92% of their initial capacity after 1000 cycles at 1 C. In contrast, anodes containing x-PAA degrade faster than the CMC reference, exhibiting about 87% of the initial capacity at the same rate and after the same number of cycles. The initial coulombic efficiencies (ICEs) are 86.2%, 87.0% and 87.1% for cells containing x-PAA, l-PAA, and CMC, respectively. Despite the different molecular structure and molecular weight of the binders, the ICEs remain very similar. This is attributed to the fact that ICE is primarily governed by the active material, and, since both the graphite and electrolyte are identical in all cells, the ICE is largely unaffected by the binder. The binder does not alter the intrinsic electrolyte reduction reactions (SEI formation) but may slightly modulate the fraction of graphite surface exposed to the electrolyte, contributing to minor variations in ICE [54].

While the adsorbed polymer layer may hinder rate performance, it plays a beneficial role during prolonged cycling by shielding the graphite surface. In x-PAA anodes, the absence of such surface coverage increases the susceptibility of the active material to irreversible lithium loss due to ongoing SEI formation. This phenomenon is likely a contributing factor to the accelerated capacity degradation observed in x-PAA cells during long-term cycling. Other possible causes of capacity loss include lithium plating or electrically isolated active material.

Cells incorporating anodes with l-PAA show a significantly lower initial capacity, approximately 2 mAh less, than those utilizing CMC and x-PAA. Furthermore, these l-PAA cells exhibit a substantially stronger capacity decay during cycling, reaching 80% of capacity retention already after 415 cycles at 1 C rate. The data for C/10 (within the check-up every 100 cycles) (Figure 7a) shows a very similar trend in capacity decay as the continuous 1 C cycling capacity fade, suggesting that the capacity decay is a true loss of active lithium and not an effect of overpotential. The internal resistance measurements are

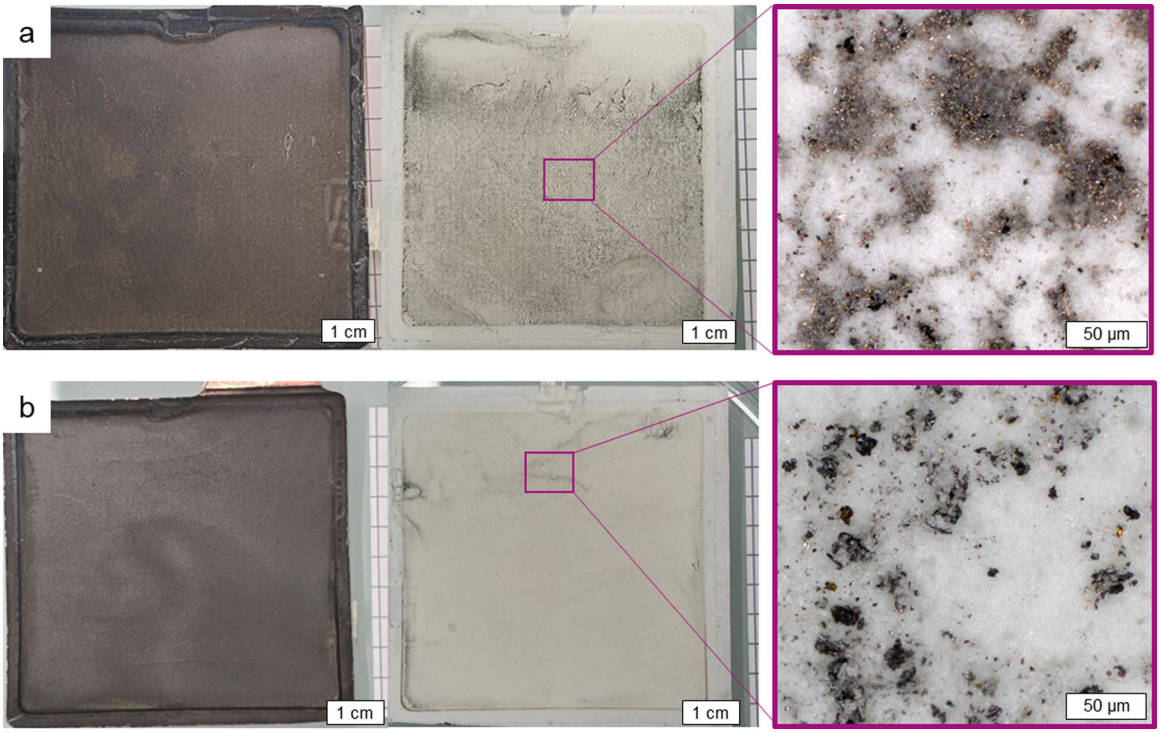

FIGURE 6 | Anodes (left column) with CMC (a) and x-PAA (b) binder, and separators (middle and right columns) from the pouch cells disassembled after rate capability test in charge direction. CMC, carboxymethyl cellulose; PAA, polyacrylic acid.

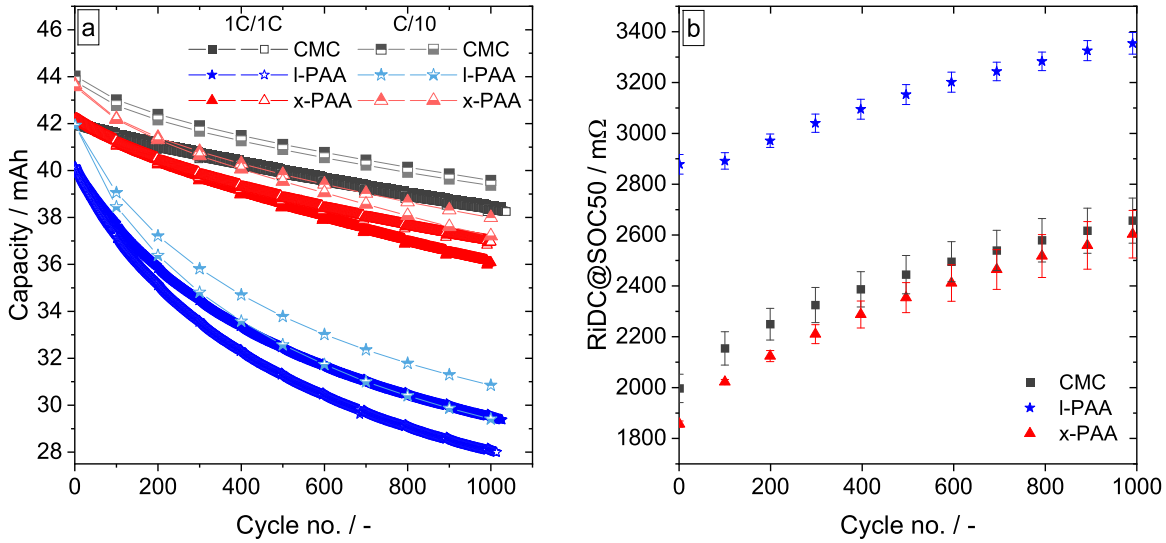

FIGURE 7 | Discharge capacity over cycles during 1C/1C charge/discharge (dark colors) and C/10 check-up cycles (light colors) (a); evolution of internal resistance (RiDC) at 50% SOC (b) for two pouch cells of each anode formulation. Each point in (b) is the average internal resistance value of two cells with anodes of one formulation. CMC, carboxymethyl cellulose; PAA, polyacrylic acid; SOC, state of charge.

presented in Figure 7b at a state of charge (SOC) of 50%. As expected, the RiDC increases for all cells throughout cycling. Due to the higher content of inactive materials, anodes with l-PAA exhibit the highest absolute internal resistance. In contrast, anodes based on x-PAA, which contain the lowest total binder content, demonstrate the lowest RiDC values.

To obtain a comprehensive understanding of the slightly diminished cycle stability in terms of capacity retention of cells containing x-PAA anodes compared to CMC reference cells, it is necessary to analyse the electrochemical data in conjunction with the post-mortem analysis data presented below.

After 1000 cycles, all cells were discharged and disassembled. The anodes and separators were then rinsed with DMC, dried, and optically inspected. The presence of lithium plating, characterized by silver-grey surface deposits on the anode surface and metallic particles on separators, can be identified only on anodes incorporating l-PAA (see Supporting Information: Figure S4). Furthermore, the separators from the cells containing x-PAA and CMC anodes exhibit only minor differences in the quantity of black particle residue, with those from the x-PAA cells exhibiting slightly higher particle accumulation than the CMC reference.

Subsequently, cycled and washed anodes were dried overnight in an oven and subjected to 90°-peel test. A comparison of the pre- and post-cycle line loads of the anodes of each formulation is illustrated in Supporting Information Figure S5. A significant decline in line load was observed in all electrodes. However, this effect is more pronounced for the CMC anode than for the two PAA based anodes. An examination of the peeled foils again reveals that while the CMC reference indicates clear adhesive failure, cohesive failure is predominant in the case of the x-PAA anodes.

To summarize, electrochemical data obtained from prolonged cycling, when evaluated in conjunction with post-mortem analyses, suggest a consistent mechanism underlying the distinct long-term cycling performance of x-PAA cells compared with the CMC references. Both, post-mortem optical inspection and peel tests indicate that the reduced performance in terms of capacity retention of x-PAA anodes may be attributed to inadequate cohesion of the electrodes. The low amount of non-adsorbing x-PAA binder is unable to fully accommodate the volume changes of the graphite particles due to de-/lithiation. In alignment with the capacity fading being similar at C/10 and 1C, most likely, the greater loss of capacity during long-term cycling for x-PAA containing anodes is due to the electric contact loss of active material.

4 | Conclusions

In this study, a highly cross-linked commercial acrylate polymer x-PAA Carbopol® Ultrez 10 (Lubrizol, USA) was utilized as a binder for aqueous-processed graphite anodes. This allowed a substantial reduction of polymeric binder concentration in the anode slurry as well as in the dry electrode layer for two reasons:

i. Due to the high thickening efficiency of this acrylate polymer with its specific heterogeneous gel structure in neutralized aqueous slurries [37], the amount of polymer required for dispersing the active material particles and thickening of the slurry could be reduced without loss in high-shear viscosity. Additionally, x-PAA provides a significant yield stress, which is advantageous for both slurry stability and the formation of well-defined electrode edges during coating.

ii. In contrast to CMC, this acrylate polymer does not adsorb on the graphite particles and thus does not disturb the adhesion between the active material and current collector foil provided by the additionally included soft SBR rubber particles [15]. This resulted in similar line load values as those measured for CMC anode layers but at significantly lower SBR content.

Based on these approaches, the total binder concentration in the dry anode layer was reduced by almost 40 wt%. However, the reduced polymer content leads to a loss of cohesion. As a result, the failure mode in peel tests is pre-dominantly cohesive for the x-PAA anode, whereas adhesive failure dominates for CMC-based anodes, as well as for another reference anode including a much higher amount of linear polyacrylic acid (l-PAA), which was necessary to adjust the processability of the corresponding slurry.

The performance of graphite anodes utilizing x-PAA was evaluated in comparison to two reference formulations employing CMC and l-PAA, respectively.

The x-PAA anode exhibited a faster capacity fading during prolonged cycling compared to the CMC reference. After 1000 cycles, cells with x-PAA demonstrate 87% of their initial capacity, whereas reference cells with CMC show 92% of capacity retention. This is attributed to the reduced cohesive strength of the anode layer. Pouch cells comprising anodes with l-PAA demonstrated the highest internal resistance due to their high binder content, and the worst cycling performance of all cells, reaching 80% of capacity retention already after 415 cycles. This phenomenon was attributed to the irreversible lithium loss resulting from plating, as revealed through post-mortem analysis.

Furthermore, anodes formulated with x-PAA binder exhibit superior charging rate performance, which is attributed to the absence of an adsorbed polymer layer on the graphite particles, enabling more effective Li^+ insertion and extraction, unlike in anodes incorporating CMC or l-PAA. Notably, CMC-based negative electrodes displayed significant lithium plating after the rate capability test in the charging direction, whereas no lithium deposits were observed in x-PAA-based anodes.

Conclusively, x-PAA proves to be a highly effective binder for graphite anodes, enabling significant reduction of inactive material content. Cells comprising anodes with x-PAA outperform those with CMC and l-PAA under fast-charging conditions. However, a trade-off with long-term cycling stability must be considered. The commercial availability of x-PAA may facilitate cost reduction and enable rapid scaling up of electrode production in comparison to costly, synthetically produced, and non-commercialized polymers. Future efforts should focus on tailoring the molecular architecture of the binder system, including the degree and distribution of crosslinking, as well as fine-tuning the mechanical properties of the electrode layer in terms of adhesion and cohesion. Presumably, the cohesion-related deficit of the x-PAA anode investigated here could be remedied by using an acrylic acid co-polymer with optimized crosslink architecture, providing similar flow behavior at slightly higher polymer concentration.

Acknowledgements

The pouch cell assembly was done at KIT Battery Technology Center (KIT-BATEC). This study contributes to the research performed at the Center for Electrochemical Energy Storage Ulm & Karlsruhe (CELEST). We thank Olivia Wiegand for support in pouch cell manufacturing and Marcus Müller for electrode calendering. Many thanks also to Stefan Heißler (Institute of Functional Interfaces, KIT) for conducting the IR spectroscopy measurements and analysis. This study was partly supported by the German Research Foundation, grant no. WI 3138/33–1. Open Access funding enabled and organized by Projekt DEAL.

Conflicts of Interest

The authors declare no conflicts of interest.

Data Availability Statement

The data supporting the findings of this study are available within this Article and the Supplementary Information file. Further data are available from the corresponding author upon request. The data that support the findings of this study are available from the corresponding author upon reasonable request.

References

1. A. Guerfi, M. Kaneko, M. Petitclerc, M. Mori, and K. Zaghib, "$LiFePO_4$ Water-Soluble Binder Electrode for Li-Ion Batteries," *Journal of Power Sources* 163 (2007): 1047–1052, https://doi.org/10.1016/j.jpowsour.2006.09.067.

2. J.-H. Lee, J.-S. Kim, Y. C. Kim, et al., "Effect of Carboxymethyl Cellulose on Aqueous Processing of $LiFePO_4$ Cathodes and Their Electrochemical Performance," *Electrochemical and Solid-State Letters* 11 (2008): A175, https://doi.org/10.1149/1.2966286.

3. A. Cholewinski, P. Si, M. Uceda, M. Pope, and B. Zhao, "Polymer Binders: Characterization and Development Toward Aqueous Electrode Fabrication for Sustainability," *Polymers* 13 (2021): 631, https://doi.org/10.3390/polym13040631.

4. B. Lestriez, "Functions of Polymers in Composite Electrodes of Lithium Ion Batteries," *Comptes Rendus Chimie* 13 (2010): 1341–1350, https://doi.org/10.1016/j.crci.2010.01.018.

5. N. Loeffler, T. Kopel, G.-T. Kim, and S. Passerini, "Polyurethane Binder for Aqueous Processing of Li-Ion Battery Electrodes," *Journal of the Electrochemical Society* 162 (2015): A2692–A2698, https://doi.org/10.1149/2.0641514jes.

6. R. Gordon, R. Orias, and N. Willenbacher, "Effect of Carboxymethyl Cellulose on the Flow Behavior of Lithium-Ion Battery Anode Slurries and the Electrical as Well as Mechanical Properties of Corresponding Dry Layers," *Journal of Materials Science* 55 (2020): 15867–15881, https://doi.org/10.1007/s10853-020-05122-3.

7. M. J. Jolley, T. S. Pathan, C. Jenkins, and M. J. Loveridge, "Exploration of High and Low Molecular Weight Polyacrylic Acids and Sodium Polyacrylates as Potential Binder System for Use in Silicon Graphite Anodes," *ACS Applied Energy Materials* 8 (2025): 1647–1660, https://doi.org/10.1021/acsaem.4c02672.

8. T. Mori and K. Kitamura, "Effect of Adsorption Behaviour of Polyelectrolytes on Fluidity and Packing Ability of Aqueous Graphite Slurries," *Advanced Powder Technology* 28 (2017): 280–287, https://doi.org/10.1016/j.apt.2016.10.005.

9. W. J. Chang, G. H. Lee, Y. J. Cheon, et al., "Direct Observation of Carboxymethyl Cellulose and Styrene–Butadiene Rubber Binder Distribution in Practical Graphite Anodes for Li-Ion Batteries," *ACS Applied Materials & Interfaces* 11 (2019): 41330–41337, https://doi.org/10.1021/acsami.9b13803.

10. T. Kwon, J. W. Choi, and A. Coskun, "The Emerging Era of Supramolecular Polymeric Binders in Silicon Anodes," *Chemical Society Reviews* 47 (2018): 2145–2164, https://doi.org/10.1039/c7cs00858a.

11. J. H. Lee, U. Paik, V. A. Hackley, and Y. M. Choi, "Effect of Carboxymethyl Cellulose on Aqueous Processing of Natural Graphite

Negative Electrodes and Their Electrochemical Performance for Lithium Batteries," *Journal of the Electrochemical Society* 152, no. 9 (2005): A1763, https://doi.org/10.1149/1.1979214.

12. X. Qi, W. Song, and J. Shi, "Density Functional Theory Study the Effects of Oxygen-Containing Functional Groups on Oxygen Molecules and Oxygen Atoms Adsorbed on Carbonaceous Materials," *PLoS One* 12 (2017): e0173864, https://doi.org/10.1371/journal.pone.0173864.

13. A. Magasinski, B. Zdyrko, I. Kovalenko, et al., "Toward Efficient Binders for Li-Ion Battery Si-Based Anodes: Polyacrylic Acid," *ACS Applied Materials & Interfaces* 2 (2010): 3004–3010, https://doi.org/10.1021/am100871y.

14. D. Mazouzi, Z. Karkar, C. Reale Hernandez, et al., "Critical Roles of Binders and Formulation At Multiscales of Silicon-Based Composite Electrodes," *Journal of Power Sources* 280 (2015): 533–549, https://doi.org/10.1016/j.jpowsour.2015.01.140.

15. K. Hofmann and N. Willenbacher, "How Carboxymethylcellulose Adsorption and Porous Active Material Particles Diminish the Adhesion of Graphite-Silicon Anodes in Lithium-Ion Batteries," *Energy Materials* 5 (2025): 500092, https://doi.org/10.20517/energymater.2024.281.

16. D. G. Mintis and V. G. Mavrantzas, "Effect of pH and Molecular Length on the Structure and Dynamics of Short Poly(Acrylic Acid) in Dilute Solution: Detailed Molecular Dynamics Study," *Journal of Physical Chemistry B* 123 (2019): 4204–4219, https://doi.org/10.1021/acs.jpcb.9b01696.

17. D. Martins, F. Dourado, and M. Gama, "Effect of Ionic Strength, pH and Temperature on the Behaviour of Re-Dispersed BC:CMC - A Comparative Study With Xanthan Gum," *Food Hydrocolloids* 135 (2023): 108163, https://doi.org/10.1016/j.foodhyd.2022.108163.

18. S. Kobayashi and K. Müllen, *Encyclopedia of Polymeric Nanomaterials* (Springer Berlin Heidelberg, 2015), https://doi.org/10.1007/978-3-642-29648-2.

19. W. Kam, C.-W. Liew, J. Y. Lim, and S. Ramesh, "Electrical, Structural, and Thermal Studies of Antimony Trioxide-Doped Poly(Acrylic Acid)-Based Composite Polymer Electrolytes," *Ionics* 20 (2014): 665–674, https://doi.org/10.1007/s11581-013-1012-0.

20. J. Wang, Q. Zheng, M. Fang, S. Ko, Y. Yamada, and A. Yamada, "Concentrated Electrolytes Widen the Operating Temperature Range of Lithium-Ion Batteries," *Advancement of Science* 8 (2021): 2101646, https://doi.org/10.1002/advs.202101646.

21. R. Xie, A. R. Weisen, Y. Lee, et al., "Glass Transition Temperature From the Chemical Structure of Conjugated Polymers," *Nature Communications* 11 (2020): 893, https://doi.org/10.1038/s41467-020-14656-8.

22. K. Hofmann, A. D. Hegde, X. Liu-Theato, R. Gordon, A. Smith, and N. Willenbacher, "Effect of Mechanical Properties on Processing Behavior and Electrochemical Performance of Aqueous Processed Graphite Anodes for Lithium-Ion Batteries," *Journal of Power Sources* 593 (2024): 233996, https://doi.org/10.1016/j.jpowsour.2023.233996.

23. R. Kasinathan, M. Marinaro, P. Axmann, and M. Wohlfahrt–Mehrens, "Influence of the Molecular Weight of Poly-Acrylic Acid Binder on Performance of Si-Alloy/Graphite Composite Anodes for Lithium-Ion Batteries," *Energy Technology* 6 (2018): 2256–2263, https://doi.org/10.1002/ente.201800302.

24. P. Parikh, M. Sina, A. Banerjee, et al., "Role of Polyacrylic Acid (PAA) Binder on the Solid Electrolyte Interphase in Silicon Anodes," *Chemistry of Materials* 31 (2019): 2535–2544, https://doi.org/10.1021/acs.chemmater.8b05020.

25. C. Li, T. Shi, H. Yoshitake, and H. Wang, "Improved Performance in Micron-Sized Silicon Anodes by In Situ Polymerization of Acrylic Acid-Based Slurry," *Journal of Materials Chemistry A* 4 (2016): 16982–16991, https://doi.org/10.1039/C6TA05650D.

26. W. Yi, T. Zhao, D. Li, et al., "Research Progress of Polyacrylate Binders for Silicon-Based Anodes In Lithium-Ion Batteries," *Chemistry – A European Journal* 31 (2025): e202500321, https://doi.org/10.1002/chem.202500321.

27. L. Wei, C. Chen, Z. Hou, and H. Wei, "Poly (Acrylic Acid Sodium) Grafted Carboxymethyl Cellulose as a High Performance Polymer Binder for Silicon Anode in Lithium Ion Batteries," *Scientific Reports* 6 (2016): 19583, https://doi.org/10.1038/srep19583.

28. Q. Huang, C. Wan, M. Loveridge, and R. Bhagat, "Partially Neutralized Polyacrylic Acid/Poly(Vinyl Alcohol) Blends as Effective Binders for High-Performance Silicon Anodes in Lithium-Ion Batteries," *ACS Applied Energy Materials* 1 (2018): 6890–6898, https://doi.org/10.1021/acsaem.8b01277.

29. Y. Gao, X. Qiu, X. Wang, et al., "Chitosan- *g* -Poly(Acrylic Acid) Copolymer and Its Sodium Salt as Stabilized Aqueous Binders for Silicon Anodes in Lithium-Ion Batteries," *ACS Sustainable Chemistry & Engineering* 7 (2019): 16274–16283, https://doi.org/10.1021/acssuschemeng.9b03307.

30. X. Zhao, C.-H. Yim, N. Du, and Y. Abu-Lebdeh, "Crosslinked Chitosan Networks as Binders for Silicon/Graphite Composite Electrodes in Li-Ion Batteries," *Journal of the Electrochemical Society* 165 (2018): A1110–A1121, https://doi.org/10.1149/2.114805jes.

31. L. Zhu, F. Du, Y. Zhuang, et al., "Effect of Crosslinking Binders on Li-Storage Behavior of Silicon Particles as Anodes for Lithium Ion Batteries," *Journal of Electroanalytical Chemistry* 845 (2019): 22–30, https://doi.org/10.1016/j.jelechem.2019.05.019.

32. H. Zhong, J. He, and L. Zhang, "Crosslinkable Aqueous Binders Containing Arabic Gum-Grafted-Poly (Acrylic Acid) and Branched Polyols for Si Anode of Lithium-Ion Batteries," *Polymer* 215 (2021): 123377, https://doi.org/10.1016/j.polymer.2020.123377.

33. A. N. Preman, S. Aswale, T. T. Salunkhe, et al., "Better Together: Integrating Adhesion and Ion Conductivity in Composite Binders for High-Performance Silicon Anodes," *Journal of Materials Chemistry A* 13 (2025): 8355–8367, https://doi.org/10.1039/D4TA07078J.

34. D. Jeong, J. Yook, D. S. Kwon, J. Shim, and J. C. Lee, "Interweaving Elastic and Hydrogen Bond-Forming Polymers Into Highly Tough and Stress-Relaxable Binders for High-Performance Silicon Anode in Lithium-Ion Batteries," *Advanced Science* 10 (2023): 2302027, https://doi.org/10.1002/advs.202302027.

35. C. Wang, S. Wu, and J. Weng, "Integrating With a Tough Framework and Efficient Self-Healing Behavior Based on a Flexible Polymer Skeleton for Si Anode Binders in Lithium-Ion Cells," *Journal of Energy Storage* 80 (2024): 110314, https://doi.org/10.1016/j.est.2023.110314.

36. P. Lv, H. Liu, Z. Cui, et al., "Covalently Cross-Linked Waterborne Polyurethane Acrylate Network Binder for Low-Expansion Silicon/Carbon Anode," *Journal of Power Sources* 655 (2025): 237985, https://doi.org/10.1016/j.jpowsour.2025.237985.

37. C. Oelschlaeger, J. Marten, F. Péridont, and N. Willenbacher, "Imaging of the Microstructure of Carbopol Dispersions and Correlation With Their Macroelasticity: A Micro- and Macrorheological Study," *Journal of Rheology* 66 (2022): 749–760, https://doi.org/10.1122/8.0000452.

38. L. Baudonnet, J. L. Grossiord, and F. Rodriguez, "Effect of Dispersion Stirring Speed on the Particle Size Distribution and Rheological Properties of Three Carbomers," *Journal of Dispersion Science and Technology* 25 (2004): 183–192, https://doi.org/10.1081/DIS-120030665.

39. A. Kowalczyk, C. Oelschlaeger, and N. Willenbacher, "Visualization of Micro-Scale Inhomogeneities in Acrylic Thickener Solutions: A Multiple Particle Tracking Study," *Polymer* 58 (2015): 170–179, https://doi.org/10.1016/j.polymer.2014.12.041.

40. J. H. Park, S. H. Kim, and K. H. Ahn, "Role of Carboxymethyl Cellulose Binder and Its Effect on the Preparation Process of Anode Slurries for Li-Ion Batteries," *Colloids and Surfaces, A: Physicochemical and Engineering Aspects* 664 (2023): 131130, https://doi.org/10.1016/j.colsurfa.2023.131130.

41. J.-H. Lee, U. Paik, V. A. Hackley, and Y.-M. Choic, "Effect of Carboxymethyl Cellulose on Aqueous Processing," *Journal of the Electrochemical Society* 152 (2005): A1763, https://doi.org/10.1149/1.1979214.

42. J. H. Park, S. H. Kim, and K. H. Ahn, "Role of Carboxymethyl Cellulose Binder and Its Effect on the Preparation Process of Anode Slurries for Li-Ion Batteries," *Colloids and Surfaces, A: Physicochemical and Engineering Aspects* 664 (2023): 131130, https://doi.org/10.1016/j.colsurfa.2023.131130.

43. J. Mewis and N. J. Wagner, *Colloidal Suspension Rheology* (Cambridge University Press, 2011), https://doi.org/10.1017/CBO9780511977978.

44. K. Dyhr and N. Willenbacher, "Formulating Graphite-Filled PU Dispersions With Extended Shelf Life Using the Capillary Suspension Concept," *Colloids and Interfaces* 9 (2025): 26, https://doi.org/10.3390/colloids9030026.

45. N. J. Balmforth, I. A. Frigaard, and G. Ovarlez, "Yielding to Stress: Recent Developments in Viscoplastic Fluid Mechanics," *Annual Review of Fluid Mechanics* 46 (2014): 121–146, https://doi.org/10.1146/annurev-fluid-010313-141424.

46. A. N. Beris, J. A. Tsamopoulos, R. C. Armstrong, and R. A. Brown, "Creeping Motion of a Sphere Through a Bingham Plastic," *Journal of Fluid Mechanics* 158 (1985): 219–244, https://doi.org/10.1017/S0022112085002622.

47. B. Bitsch, J. Dittmann, M. Schmitt, P. Scharfer, W. Schabel, and N. Willenbacher, "A Novel Slurry Concept for the Fabrication of Lithium-Ion Battery Electrodes With Beneficial Properties," *Journal of Power Sources* 265 (2014): 81–90, https://doi.org/10.1016/j.jpowsour.2014.04.115.

48. B. G. Westphal and A. Kwade, "Critical Electrode Properties and Drying Conditions Causing Component Segregation in Graphitic Anodes for Lithium-Ion Batteries," *Journal of Energy Storage* 18 (2018): 509–517, https://doi.org/10.1016/j.est.2018.06.009.

49. B. Westphal, H. Bockholt, T. Günther, W. Haselrieder, and A. Kwade, "Influence of Convective Drying Parameters on Electrode Performance and Physical Electrode Properties," *ECS Transactions* 64 (2015): 57–68, https://doi.org/10.1149/06422.0057ecst.

50. J. Kumberg, W. Bauer, J. Schmatz, et al., "Reduced Drying Time of Anodes for Lithium-Ion Batteries Through Simultaneous Multilayer Coating," *Energy Technology* 9 (2021): 2100367, https://doi.org/10.1002/ente.202100367.

51. A. Smith, P. Stüble, L. Leuthner, A. Hofmann, F. Jeschull, and L. Mereacre, "Potential and Limitations of Research Battery Cell Types for Electrochemical Data Acquisition," *Batter. Supercaps* 6 (2023): e202300080, https://doi.org/10.1002/batt.202300080.

52. R. Tian, S.-H. Park, P. J. King, et al., "Quantifying the Factors Limiting Rate Performance in Battery Electrodes," *Nature Communications* 10 (2019): 1933, https://doi.org/10.1038/s41467-019-09792-9.

53. R. Gordon and A. Smith, "Towards More Realistic Li-Ion Battery Safety Tests Based on Li-Plating as Internal Cell Error," *Journal of Energy Storage* 72 (2023): 108200, https://doi.org/10.1016/j.est.2023.108200.

54. K. Ui, D. Fujii, Y. Niwata, et al., "Analysis of Solid Electrolyte Interface Formation Reaction and Surface Deposit of Natural Graphite Negative Electrode Employing Polyacrylic Acid as a Binder," *Journal of Power Sources* 247 (2014): 981–990, https://doi.org/10.1016/j.jpowsour.2013.08.083.

Supporting Information

Additional supporting information can be found online in the Supporting Information section.
SI Cross-Linked Acrylate Binder for High-Rate Graphite Anodes 08092025.